Mixing of argon-ion and carbon dioxide laser radiation in uniaxial rubidium chlorate crystals*

D. M. Hwang and S. A. Solin
The Department of Physics and the James Franck Institute, The University of Chicago, Chicago, Illinois 60637
(Received 24 September 1973)

Mixing in uniaxial $RbClO_3$ of visible and infrared photons emitted, respectively, by an argon-ion and CO_2 laser has been examined at room temperature under conditions in which the two laser beams propagate collinearly in the single crystal. The intensity dependence of the Stokes (down-converted) and anti-Stokes (up-converted) mixed-phonon signals has been measured as a function of the propagation direction of the collinear CO_2 and argon-ion laser beams and has been found to vary by three orders of magnitude as θ, the angle between the wave vector of the visible (or infrared) laser beam and the crystal c axis varies from 0° to 90°. The mixed-photon signal intensity achieves its maximum value at a critical propagation angle θ_c at which phase matching is achieved. The functional dependence of θ_c on the CO_2-laser wavelength has been calculated and measured. The excellent agreement between experiment and theory provides an additional, yet independent, check of the dielectric functions of $RbClO_3$ which have been determined previously from Raman scattering measurements. The polarization relationships between the mixed photons and the incident photons have been studied carefully and analyzed through both the second-order nonlinear susceptibility tensor and the Raman tensors. Group-theoretically-derived polarization selection rules are rigorously obeyed as evidenced by experimental depolarization factors in excess of 1000. Consistent with wave-vector selection rules, the mixed photons that emerge from the $RbClO_3$ crystal are highly collimated along a specified direction. The mixing process, in addition to being viewed as a second-order nonlinear interaction, is treated as Raman scattering from angular-tunable optically pumped hot phonons and polaritons. Nonequilibrium steady-state pumped-polariton gains in excess of 10^8 corresponding to equilibrium sample temperatures of the order of 10^{11} °K have beem measured and calculated. An extensive search was made for first- and second-order Raman scattering from the hot-polariton decay and scattering products. No such damping products were observed for reasons related principally to limitations in the minimum achievable measurement temperature.

I. INTRODUCTION

In a recent letter[1] (hereinafter designated I) we reported briefly the mixing in $RbClO_3$ of visible and infrared radiation emitted by an argon-ion and CO_2 laser, respectively. Our purpose in this paper is to present a complete analysis of the $RbClO_3$ mixing experiment, including hitherto unreported aspects of the polarization properties of the output radiation.

The mixing process can be described either in terms of sum and difference frequency generation via the second-order nonlinear susceptibility or as Stokes and anti-Stokes Raman scattering from optically pumped hot phonons and polaritons. While the literature is replete with reports of nonlinear mixing experiments, investigations reported to date have dealt almost exclusively with the mixing of photons to which the nonlinear medium is transparent. On the other hand, Faust and Henry[2] and Faust *et al.*[3] have successfully used GaP to mix the visible 6328-Å radiation of a He-Ne laser with several of the lines of an H_2O laser covering a range from ~23–50 μm and including one line at 26.660 μm which is strongly absorbed in GaP. Thus Faust and his co-workers were able to determine the frequency dispersion in the second-order nonlinear susceptibility of GaP, particularly in a region of high dispersion coinciding with the region of high absorption. The CO_2-laser emission lines do not span a large enough wavelength range to allow us to determine definitively the frequency dispersion of the second-order nonlinear susceptibility of $RbClO_3$. We shall, however, discuss in detail directional dispersion, an additional dispersive property which is absent from cubic crystals such as GaP.

It was pointed out in I that GaP is, from the point of view of its linear and nonlinear susceptibilities as well as its polariton properties, a very simple crystal; it is cubic with two atoms per primitive cell[4] and thus exhibits no directional dispersion in its phonon or polariton frequencies. In contrast $RbClO_3$ is trigonal uniaxial with five atoms per cell.[5] All of the seven Raman-active phonons in this material are polar; both the phonons and polaritons exhibit large directional dispersion.[6] Whereas the nonlinear susceptibility of GaP is discrete, we can characterize the nonlinear susceptibility of $RbClO_3$ as angular tunable, i.e., the dispersion of the second-order nonlinear susceptibility associated with a given polariton branch in $RbClO_3$ is a function of the polariton propagation direction in the crystal. We will show in this paper that the

directional dispersion can be usefully employed to extract valuable information on the polariton spectrum of a uniaxial material and can also serve as a check of the dielectric functions.

As a byproduct of the mixing experiment described above, we have searched extensively for the decay products of the hot phonons and polaritons, decay products which were expected to result from the anharmonic three-phonon interaction. No such decay products were observable, for reasons which shall be discussed.

II. EXPERIMENTAL APPARATUS

Figure 1 shows a block diagram of the apparatus used in the mixing experiment. The output of a Coherent Radiation Laboratories model 52A argon-ion laser is apertured by diaphrams D_1 and D_2 and deflected by a pair of Pellin Brocca constant-deviation prisms. These prisms, which are manually adjustable, were used to spatially disperse unwanted fluorescence emission from the laser. The argon-laser beam, after reflecting from mirror M_1, is, upon a second reflection, merged collinearly by dichroic mirror P_1 with the output of a Q-switched CO_2 laser. The mirror P_1 transmits over 90% of the CO_2 beam while simultaneously reflecting over 95% of the argon beam. The collinear argon- and CO_2-laser beams pass through apertures D_3 and D_4, beam splitter P_2 and aperture D_5. A barium fluoride flat is used for beam splitter P_2 and reflects ~10% of the incident (visible or ir) radiation while transmitting ~85%. Upon emerging from aperature D_5, the collinear beams reflect off of a plane mirror M_2 and are focused by spherical mirror M_3 (focal length = 20 cm) onto the $RbClO_3$ sample. A second barium fluoride beam splitter P_3 is used in conjunction with filter P_4 and a Coherent Radiation Laboratories model 210 thermopile detector coupled to a Kiethly model 150 B microvoltmeter to monitor the average CO_2-laser power. Filter P_4 is identical in construction to the dichroic mirror P_4. Forward-Raman-scattered (frequency-mixed) Stokes (down-shifted) and anti-Stokes (up-shifted) argon-laser radiation is collected by lenses L_1 and L_2, dispersed by a Jarrel-Ash model 25-100 double monochromator equipped with a pair of 1180 groove/mm gratings blazed at 5000 Å, and detected by a cooled ITT/FW 130 phototube. When Stokes radiation is being examined, a Corning model CS3-69 long-pass filter, F in Fig. 1, is used to eliminate parasitic and Rayleigh-scattered argon-laser radiation.

The electronic detection system used to process the phototube output signal consists of a preamplifier, an amplifier, and two parallel channels, one containing a Princeton Applied Research model 160 boxcar integrator and the other a photon-counting system constructed from Ortec and Canberra components (single-channel analyzer, linear ratemeter, digital ratemeter). Preamplified trigger pulses for the boxcar integrator are derived from a Molectron model $P3$ pyroelectric detector exposed to the CO_2 laser radiation which is beam split by P_2 (see Fig. 1), focused with barium fluoride lens L_3, and dispersed with a Jarrel-Ash model 82-410 monochromator equipped with a 50-groove/mm grating blazed at 10 μm. The 82-410 monochromator was used to accurately identify the wavelength of the CO_2-laser emission line. To assure proper triggering by the pyroelectric detector, the boxcar integrator gate and trigger signals were displayed simultaneously on a Tektronix model 561B oscilloscope. A Hewlett-Packard dual-pen chart recorder synchronized with the double-monochromator drive

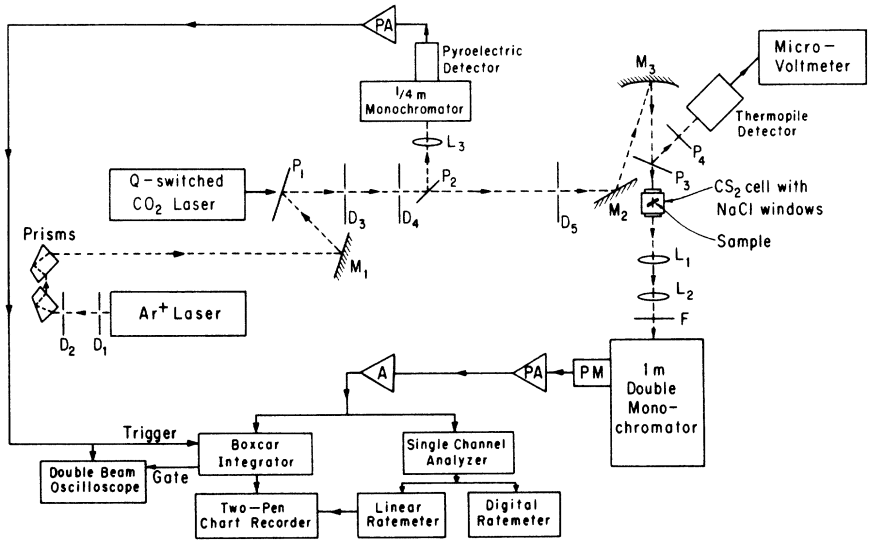

FIG. 1. Experimental setup for the mixing of Ar^+-laser visible radiation and CO_2-laser infrared radiation in $RbClO_3$.

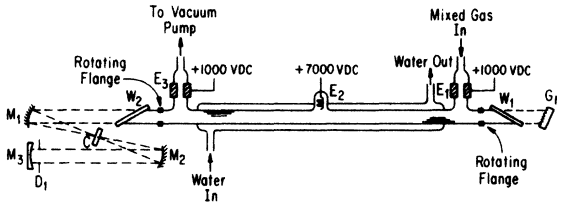

FIG. 2. The mechanically Q-switched CO_2 laser used in this experiment. A variable-speed chopper C is placed at the common focus of spherical mirrors M_1 and M_2.

system was used to display simultaneously the wavelength dependence of the boxcar and photon-counting signals. The boxcar was gated "on" for the duration of each CO_2 radiation pulse and therefore responded only to those Raman (mixing) signals with intensities modulated by the Q-switched CO_2-laser radiation. On the other hand, the photon-counting channel sensed all Raman-scattered radiation, whether modulated or not.

The CO_2 laser used in this experiment was homemade and incorporated a unique efficient, and yet inexpensive, Q-switching system compatible with single-line operation at high average powers and high repetition rates. A diagram of the optical configuration of the CO_2 laser is shown in Fig. 2. The laser tube is 1.3 m long, water cooled, and has a 1 cm bore. The ends are sealed with NaCl Brewster windows, which can be rotated about the tube axis to achieve a linearly polarized output the plane of which is variable. Typically the laser was operated with the tungsten anode at 7000 V and the nickel cathodes at ~1000 V. The cathode voltage was feedback regulated to maintain a constant discharge current which could be preset. A flowing mixture of He, N_2, and CO_2 at a total pressure of 10 torr served as the active medium. The optical cavity consisted of three mirrors and a grating arranged in a "Z" configuration as shown in Fig. 2. The two mirrors labeled M_1 and M_2 were identical and had 0.4-m radii of curvature spherical aluminized front surfaces which were overcoated with silicon monoxide. These mirrors were obtained as stock items from the Ealing Corporation for the minimal cost of $6 apiece. A 10-m radius of curvature dielectric-coated germanium mirror M_3, having a reflectivity of 85%, was used as the cavity output coupler, while a Photo Technical Research, Inc. model 1800 P grating, G_1, was used in the Littrow configuration and in conjunction with the adjustable aperature D_1 to obtain single-line operation. Q switching was accomplished by placing a variable-speed chopper at the common focus of mirrors M_1 and M_2. A Princeton Applied Research Corporation model 222 chopper, fitted with an 8-in. aluminum blade containing 48 equally spaced 0.031-in.-wide slots, was employed. The dependence of the average Q-switched single-line power on the pulse repetition rate is shown in Fig. 3, while the output pulse shape is shown in the insert of that figure. For efficient high-power cw operation, mirror M_3 was placed in the position of mirror M_1 and the grating was replaced by a high reflector ($R > 99\%$). Linearly polarized multimode all-line cw output power in excess of 80 W has been obtained with the above-described laser.

Samples of $RbClO_3$ were grown from solution using methods described in detail elsewhere.[6] The specimens examined were thin platelets of typical dimension $5 \times 3 \times 0.1$ mm. The faces of these platelets were quite rough, the major flaws being parallel closely spaced striations. To eliminate artificial depolarization and uncontrolled changes in photon propagation direction, the samples were immersed in an index-matching fluid.[7] Carbon disulfide was used for index matching because it is highly transparent to both visible and 10.6-μm ir radiation. Its absorption coefficient is negligibly small when measured with visible light and has a value of 0.26 cm^{-1} at 10.6 μm.[8] Furthermore, the index of refraction of CS_2 is 1.63 at 5893 Å,[9] a value close to the two indices of $RbClO_3$ ($n_e = 1.484$, $n_0 = 1.572$).[10] The index-matching fluid was contained in an aluminum cell fitted on opposite sides with NaCl windows which were affixed permanently to the cell with epoxy (Emerson-Cummings Stycast No. 2850 FT plus catalyst 24 LV). The sample was immersed in and attached to the sample cell in such a way as to allow the optic axis to be accurately positioned in any direction in a horizontal plane containing the unmerged CO_2- and Ar^+-laser beams.

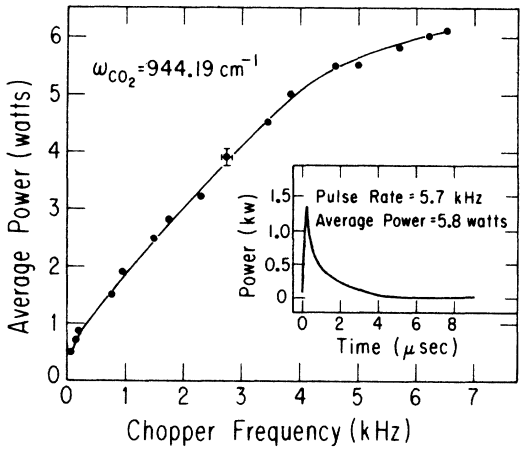

FIG. 3. The average output power of the Q-switched CO_2 laser (single line operation) as a function of the chopping frequency. The insert shows the trace of the pulse shape detected by a pyroelectric detector (time constant 50 nsec) and displayed on an oscilloscope.

The spectra reported in this paper are labeled both with the standard Raman notation $i(jk)l$ [11] and with the additional notation $m(n)$. Here i and j (l and k) represent, respectively, the propagation and polarization directions of the incident (scattered) argon-laser radiation, while m and n correspond to the propagation and polarization directions of the CO_2-laser radiation. Thus the designation $i(jk)l;\ m(n)$ specifies a measurement both of the Raman tensor component α_{jk} and the second-order nonlinear susceptibility tensor component d_{kjn}. While the primitive unit cell of $RbClO_3$ is rhombohedral, it is convenient to label spectra by the orthogonal axes defined by Nye[12] for the hexagonal unit cell, i.e., $i, j, k, l, m, n, = x, y,$ or z.

III. RESULTS AND DISCUSSION

A. Sample spectra

An example of a down-converted Stokes Raman signal is shown in Fig. 4, which is a reproduction of the dual-pen recorder tracing. The broad peak centered at ~920 cm^{-1} in the recorder trace of the photon-counting channel corresponds to spontaneous Raman scattering from a thermal polariton, the breadth of which is attributable to the large collection aperture used to record the spectrum. The sharp peak at 946 cm^{-1} arises from the down-shifted photon produced in the mixing experiment or, equivalently, from spontaneous Stokes Raman scattering from hot polaritons pumped by the 946 cm^{-1} $p(30)$ line of the CO_2 laser.[13] As expected, the boxcar channel senses only that part of the scattered signal modulated by the CO_2-laser Q-switch pulse, while the photon-counting channel responds to both modulated and unmodulated Raman signals. In order to facilitate a comparison of the hot- and thermal-polariton signals, an inefficient scattering geometry was used to record the data of Fig. 4. As will be seen shortly, down-converted photon signals, two orders of magnitude more intense than that shown in Fig. 4, have been observed.

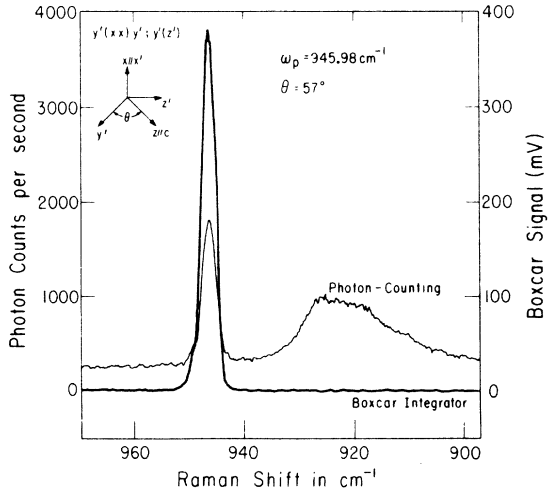

FIG. 4. Typical Stokes Raman spectrum of a $RbClO_3$ crystal pumped by the 946-cm^{-1} line of a CO_2 laser and probed by the 5145-Å argon-laser line. The boxcar integrator only recorded those signals with intensity modulated by the CO_2-laser radiation. Note that in this figure and in Figs. 5–7, 9, and 12 the abcissa is linear in wavelength rather than in wave number.

B. Polarization properties

It is instructive to deduce the polarization properties of the Raman scattered (up- or down-converted) photons from both the Raman tensors and the second-order nonlinear susceptibility tensor of $RbClO_3$. The five-atom rhombohedral primitive cell of $RbClO_3$ has space-group symmetry C_{3v}^5.[5] Crystals belonging to this symmetry class are piezoelectric and have the interesting property that all of their polar modes are Raman active while, simultaneously, all of their Raman-active modes are polar.[6] The Raman tensors corresponding to the A_1 and E species of the C_{3v} point group referred to the x, y, and z crystal axes, are given by[14]

$$A_1(z)=\begin{bmatrix} a & 0 & 0 \\ 0 & a & 0 \\ 0 & 0 & b \end{bmatrix};\quad E(y)=\begin{bmatrix} c & 0 & 0 \\ 0 & -c & d \\ 0 & d & 0 \end{bmatrix};$$

$$E(-x)=\begin{bmatrix} 0 & -c & -d \\ -c & 0 & 0 \\ -d & 0 & 0 \end{bmatrix}.$$

Letters in parentheses indicate the direction of polarization of the phonon. The nonzero tensor components, and therefore the symmetry species of the Qth normal mode, are determined from

$$P_i(\omega_S)=\sum_j \alpha_{ij}^{Qk} E_i(\omega_L). \qquad (1)$$

Here $P_i(\omega_S)$ is the ith Cartesian component of the induced polarization at the scattered frequency, ω_S, $E_i(\omega_L)$ is the ith component of the applied argon-laser electric field at frequency ω_L, and α_{ij}^{Qk} is the component of the Raman tensor associated with the irreducible representation (symmetry species) of the Qth normal mode, which is, itself, polarized in the k direction. In order to apply Eq. (1) to the mixing process one must first determine which normal modes are pumped by the CO_2 laser; i.e., a necessary condition for mixing to occur is that the electric vector of the CO_2 laser field have a nonvanishing projection in the k direction.

The polarization selection rules can also be deduced from the second-order nonlinear susceptibility tensor $\vec{d}$ using the following equation[15]:

$$P_i(\omega_S)=\sum_{jk} d_{ijk}(\omega_S=\omega_L\pm\omega_P)E_j(\omega_L)E_k(\omega_P). \qquad (2)$$

Here $E_k(\omega_P)$ is the kth Cartesian component of the CO_2 laser field at the pump frequency ω_P and the other symbols retain the definitions applied to Eq. (1). The nonlinear susceptibility tensor in its most general form is a $(3\times3\times3)$ third-rank tensor. However, there is no physical difference introduced by the interchange of the j and k subscripts[16]; thus

$$d_{ijk} \equiv d_{ikj}, \tag{3}$$

and the kj subscripts can be replaced by the single subscript l giving rise to the contracted susceptibility tensor with components d_{il}. The d_{il} tensor appropriate to $RbClO_3$ is shown in Eq. (4),[15] properly applied to the E^2 column tensor to yield the induced-polarization components P_x, P_y, P_z:

$$\begin{bmatrix} P_x \\ P_y \\ P_z \end{bmatrix} = \begin{bmatrix} 0 & 0 & 0 & 0 & d_{15} & -d_{22} \\ -d_{22} & d_{22} & 0 & d_{15} & 0 & 0 \\ d_{31} & d_{31} & d_{33} & 0 & 0 & 0 \end{bmatrix} \begin{bmatrix} E_x(\omega_L)E_x(\omega_P) \\ E_y(\omega_L)E_y(\omega_P) \\ E_z(\omega_L)E_z(\omega_P) \\ E_y(\omega_L)E_z(\omega_P)+E_y(\omega_P)E_z(\omega_L) \\ E_x(\omega_L)E_z(\omega_P)+E_x(\omega_P)E_z(\omega_L) \\ E_x(\omega_L)E_y(\omega_P)+E_x(\omega_P)E_y(\omega_L) \end{bmatrix}. \tag{4}$$

In Fig. 5 we show polarization spectra that verify the selection rules dictated by the Raman and nonlinear susceptibility tensors. Scattering attributable to the Raman tensor component α_{xx} is shown in Fig. 5(a). Raman tensors corresponding to the $A_1(z)$ and $E(y)$ modes have nonzero xx components. But the CO_2 pump photon can create only phonons or polaritons polarized in the z direction, i.e., those of A_1 symmetry. Since, by the wave-vector selection rule,[14] the hot A_1 polariton propagates in the y direction and is polarized in the z direction, it is a transverse-optical (TO) polariton.[17] Thus, in the Raman terminology, the peak at 935 cm^{-1} in Fig. 5(a) corresponds to allowed scattering from a hot A_1(TO) polariton. The broad peak centered at ~922 cm^{-1} represents allowed scattering from thermal polaritons having mixed A_1 and E symmetry. Since $RbClO_3$ sustains no phonons polarized in the z direction which are characterized by a Raman tensor with a nonzero xz component, scattering from hot phonons or polaritons is not allowed for the polarization configuration of Fig. 5(b). Indeed, even with a gain (sensitivity) increase of 20 compared with Fig. 5(a), no hot polaritons are detected. The peak at ~940 cm^{-1} in Fig. 5(b) results from thermal polaritons of E symmetry.[18]

Referring again to the polarization configuration specified in Fig. 5(a), we note that $y(xx)y$; $y(z)$ corresponds, according to Eq. (2), to a measurement of the nonlinear susceptibility tensor component d_{xxz} which is equal to d_{15} in the contracted notation.[15] Since $d_{15}\neq0$ for $RbClO_3$ [see Eq. (4)], mixing is allowed and the down-shifted photon is observed at 935 cm^{-1} in Fig. 5(a). In contrast, the polarization configuration $y(xz)y$; $y(z)$ of Fig. 5(b) indicates a measurement of the nonlinear susceptibility tensor component $d_{zxz}=d_{35}$. We note from Eq. (4) that for $RbClO_3$, $d_{35}=0$. No mixing is allowed or observed in the polarization configuration of Fig. 5(b).

A polarization analysis similar to that described above can also be applied to Figs. 5(c) and 5(d) with equally gratifying results. Whether analyzed in terms of the Raman tensors or the second-order nonlinear susceptibility tensor, the group-theoretically-determined polarization selection rules for mixing ir and visible light in $RbClO_3$ are perfectly obeyed, as evidenced by experimentally observed depolarization factors in excess of 1000 (see Fig. 5).

C. Propagation constraints

The mixing experiments described in this paper were conducted with the argon-laser probe beams and CO_2-laser pump beams propagating collinearly in the crystal. The strongly absorbed CO_2 photon propagates in the crystal as a polariton with a large spread in the magnitude of its wave vector ($|\Delta\vec{q}|\sim\alpha$, where α is the absorption coefficient in cm^{-1} at the frequency of the CO_2 photon) but with a well-defined energy and propagation direction. Since conservation of wave vector applies to the Raman process, we find

$$\vec{k}_S = \vec{k}_L \pm \vec{q}, \tag{5}$$

where $\vec{k}_L$, $\vec{k}_S$ and $\vec{q}$ are, respectively, the wave vectors (in the crystal) of the incident argon-laser photon, the scattered argon-laser photon, and the polariton. Equation (5) is satisfied only if both Stokes and anti-Stokes photons, Raman scattered from hot polaritons, propagate collinearly with the CO_2- and argon-laser beams. The propagation constraint imposed by Eq. (5) is verified in Fig. 6. Figure 6(a) was recorded with a collection aperture of $f2$ (cone angle 28°) centered about the collinear CO_2- and argon-laser beams. Both the sharp hot-polariton peak at 929 cm^{-1} and a broad peak at ~918 cm^{-1} are vislble in Fig. 6(a).

The latter peak results from thermal polaritons and is broad because of the large spread in polariton wave vector sampled with a large collection aperture. The spectrum of Fig. 6(b) was recorded

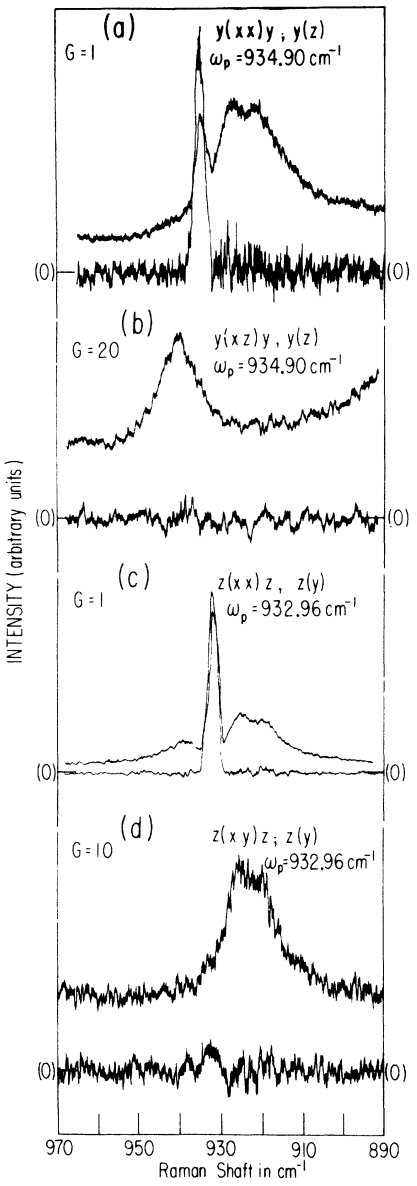

FIG. 5. Polarization study of the hot-polariton spectrum. In (a) and (b), the sharp pumped polaritons have symmetry $A_1(z)$, and exhibit a nonzero α_{xx} (d_{xxz}) Raman (nonlinear susceptibility) tensor component in (a) and a zero α_{xz} (d_{zxz}) component in (b). In (c) and (d) the sharp pumped polaritons have symmetry $E(y)$ and exhibit nonzero α_{xy} (or d_{xxy}) tensor components in (c) and zero α_{xy} (or d_{yxy}) components in (d). The broad peaks which appear only in the photon-counting channel are due to ordinary thermal polaritons which in (a) and (c) have mixed $A_1(z)+E(y)$ symmetry and have pure $E(-x)$ symmetry in (b) and (d).

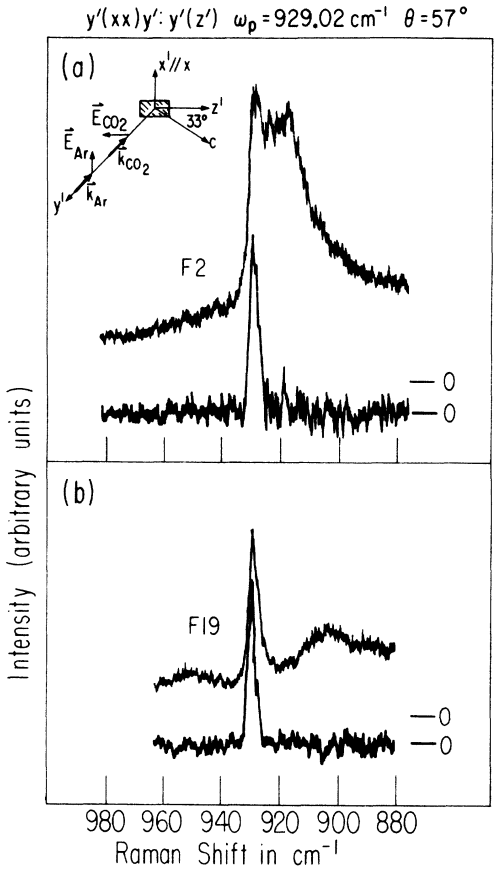

FIG. 6. Collection aperature effect on the pumped Raman spectrum. (a) and (b) were recorded with the same experimental conditions except that the collection aperture was changed from $f2$ in (a) to $f19$ in (b).

under conditions almost identical to those used in Fig. 6(a), the only difference being a reduction in collection aperture to $f19$ (cone angle 3°). Note that the hot-polariton (down-shifted photon) peak exhibits the same scattering intensity in Figs. 6(a) and 6(b), whereas the thermal polariton, as expected, shows in Fig. 6(b) a significant decrease in intensity and a shift to lower energy with decreasing aperture.

D. Intensity considerations

The intensity of the photons produced at the sum and difference frequencies $\omega_S = \omega_L \pm \omega_P$ is given by

$$I(\omega_S, \theta) = C\omega_S^4 |d(\omega_P, \theta)|^2 [l_c(\omega_P, \theta)]^2 \times [n(\omega_P, \theta)]^{-1} I(\omega_L) I(\omega_P) . \quad (6)$$

Here C is a constant, θ is the angle between $\vec{q}$ and the crystal c axis, n is the refractive index, and l_c is the coherence length and is given by

$$l_c(\omega_P, \theta) = \{[|\Delta\vec{k}(\omega_P, \theta)|]^2 + [\tfrac{1}{2}\alpha(\omega_P, \theta)]^2\}^{-1/2} . \quad (7)$$

In Eq. (7), $\alpha(\omega_P, \theta)$ is the absorption coefficient (units of cm^{-1}) and $|\Delta\vec{k}(\omega_P, \theta)|$ represents a phase mismatch, which shall be defined shortly. For a uniaxial crystal the parameters, d, l_c, and n are all θ dependent; therefore, the photon flux at ω_S is θ dependent. However, over the frequency range spanned in this experiment, ω_S and ω_L are far from resonance, and the second-order nonlinear susceptibility tensor $\vec{d}$ is an implicit function of ω_P and θ only. Therefore, we expect the Stokes (down-shifted) photon at $\omega_S = \omega_L - \omega_P$ to scatter with approximately the same intensity as the anti-Stokes photon at $\omega_S = \omega_L + \omega_P$. In Fig. 7 we show the Stokes and anti-Stokes signals created by mixing the 940-cm^{-1} line of the CO_2 laser with the 5145-Å argon-laser line. In the experimental configuration of Fig. 7, the hot-polariton signal is three orders of magnitude more intense than the thermal polariton signal; therefore, the latter is not observable on the scale of Fig. 7 (see also Fig. 12). When the spectrum of Fig. 7 is corrected for the dispersion of the instrumental transfer function,[19] we find that the experimental anti-Stokes–Stokes polariton intensity ratio

$$\left(\frac{I(\omega_S = \omega_L + \omega_P, \theta)}{I(\omega_S = \omega_L - \omega_P, \theta)}\right)_{exp} = 1.43 \pm 0.15 \quad (8)$$

is in excellent agreement with the theoretical ratio calculated from Eq. (6),

$$\left(\frac{I(\omega_S = \omega_L + \omega_P, \theta)}{I(\omega_S = \omega_L - \omega_P, \theta)}\right)_{th} = \left(\frac{\omega_L + \omega_P}{\omega_L - \omega_P}\right)^4 = 1.47 . \quad (9)$$

In terms of the Raman process, the Q-switched CO_2 photons modulate the occupation number N of the hot polaritons which they create. But the Stokes and anti-Stokes scattering intensities are proportional, respectively, to $(N+1)$ and N. For polaritons in thermal equilibrium, the boson occupation number N_E obtains and is given by

$$N_E = (e^{\hbar\omega/K_B T} - 1)^{-1} ,$$

where K_B is Boltzmann's constant and T is the absolute temperature of the crystal. At room temperature, the equilibrium value of N_E for a polariton with $\omega = 946$ cm^{-1} is 6.78×10^{-3}.

The nonequilibrium value of N, labeled N_{NE} can be estimated as follows. We assume for simplicity that all incident CO_2 photons are absorbed uniformly by the $RbClO_3$ crystal over the absorption length $1/\alpha(\omega_P, \theta)$, i.e., the photon-polariton conversion efficiency is 1 and reflection losses are negligible.[20] Typically 50 mW of focused CO_2 average pump power was applied to the $RbClO_3$ sample. Average powers in excess of that value caused the CS_2 in contact with the sample to boil. The hot-polariton steady-state nonequilibrium number density n^* produced in one absorption length of the crystal $[1/\alpha(946\ cm^{-1}, 45°) \approx 2\ \mu m$ for $RbClO_3]$ is given by

$$n^* = P(\omega_P)(1 - e^{-1})\alpha(\omega_P, \theta)\tau , \quad (10)$$

where $P(\omega_P)$ is the incident CO_2 flux in photons/sec cm^2, τ is the polariton lifetime, and e is the base for natural logarithms. For a $\omega_P = 946$ cm^{-1} 50-mW CO_2 beam focused to a spot size of 1.2 mm diam, we find, using $\alpha(946\ cm^{-1}, 45°) = 5000$ cm^{-1} and $\tau \approx 10^{-12}$ sec (Ref. 21) that $n^* \cong 1.58 \times 10^{11}$ cm^{-3}. The n^* polaritons are distributed among many modes having an approximate mode density g given by

$$g \cong \Omega[n(\omega_P, \theta)]^{-2} |\vec{q}|^2 (\Delta|\vec{q}|)(2\pi)^{-3} . \quad (11)$$

Here Ω is the solid angle (in air) subtended by the focused CO_2-laser beam. For the experimental conditions appropriate to Fig. 7 we have $\Omega = 2.5 \times 10^{-3}$ sr, $n(946\ cm^{-1}, 45°) = 1.5$, $|\vec{q}| = 1419$ cm^{-1}, $\Delta|\vec{q}| \cong 100$ cm^{-1}. Inserting these values into Eq. (11) we find $g \cong 901$ cm^{-3}. Therefore the estimated polariton nonequilibrium occupation number N_{NE} is

$$N_{NE} = n^*/g = 1.8 \times 10^8 . \quad (12)$$

For the Raman process,

$$\left(\frac{I(\omega_S = \omega_L + \omega_P, \theta)}{I(\omega_S = \omega_L - \omega_P, \theta)}\right)_{th} = \left(\frac{\omega_L + \omega_P}{\omega_L - \omega_P}\right)^4 \frac{N}{N+1} . \quad (13)$$

In the presence of CO_2 pump photons $N = N_{NE}$ and $(N_{NE} + 1)/N_{NE} \cong 1$. Equation (13) reduces to Eq. (9), as expected. The theoretical Stokes Raman signal

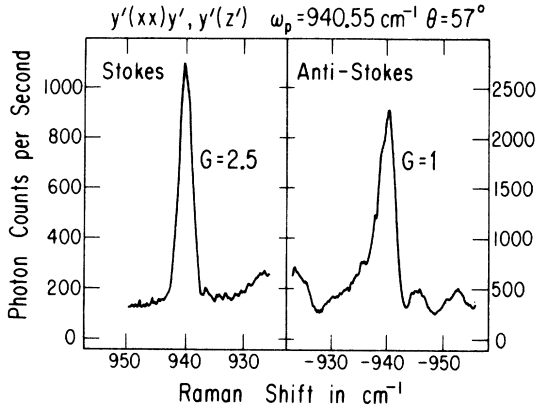

FIG. 7. Comparison of hot polariton Stokes and anti-Stokes Raman signals. Note that the Corning CS3-69 filter was not used to record the anti-Stokes spectrum. This accounts for the presence in the anti-Stokes spectrum of ghosts. The observed anti-Stokes–Stokes ratio was 2.02. After correction for the instrumental transfer function and the effect of the CS3-69 filter, the ratio was found to be 1.43 ± 0.15.

gain, G_{th}, attributable to the production of hot polaritons is

$$G_{th} = (N_{NE}+1)/(N_E+1) \approx N_{NE}\,, \tag{14}$$

so $G_{th} \cong 1.8\times10^8$ for the conditions applicable to Fig. 7. The experimental value of the signal gain, G_{exp}, involves the product of several factors, as shown in Eq. (15):

$$G_{exp} = (R_{NE}/R_E)(L_E/L_{NE})(S_E/S_{NE})(A_{CO_2}/A_{Ar^+})\,. \tag{15}$$

Here R_{NE}/R_E is the ratio of nonequilibrium and thermal Stokes polariton signals, L is the appropriate scattering length, S is an instrumental throughout factor related to the effective spectral slit width, and A is the cross-sectional area of the laser beam in the crystal. The experimental values (appropriate to Fig. 7) for the four product factors in Eq. (15) are respectively 125, 50, 300, and 36, thus $G_{exp} = 6.8\times10^7$. Given the assumptions involved in the calculation of N_{NE}, the theoretical and experimental values of G are in surprisingly good agreement.

E. Tunability and intensity measurements

Rubidium chlorate was chosen for this mixing experiment because its polariton dispersion curves exhibit directional dispersion and, in addition, span a frequency range in which the CO_2 laser emits many discrete lines. The dielectric functions of $RbClO_3$ as well as the directional dispersions of all the phonon modes have been previously determined experimentally and have been calculated from Raman measurements of the frequencies of the seven pairs of TO and LO phonons.[6] The undamped polariton directional dispersion curves are given by[22]

$$|\vec{q}(\omega,\theta)|^2 = \omega^2\left(\frac{\sin^2\theta}{\epsilon_\infty^{\parallel}}\prod_{i=1}^{3}\frac{(\omega_{iA_1}^{TO})^2-\omega^2}{(\omega_{iA_1}^{LO})^2-\omega^2} + \frac{\cos^2\theta}{\epsilon_\infty^{\perp}}\prod_{i=1}^{4}\frac{(\omega_{iE}^{TO})^2-\omega^2}{(\omega_{iE}^{LO})^2-\omega^2}\right)^{-1}. \tag{16}$$

Here ω, q, and θ are, respectively, the polariton frequency, wave vector, and propagation angle with respect to the crystal c axis; $\epsilon_\infty^{\parallel}$ ($\epsilon_\infty^{\perp}$) is the high-frequency dielectric constant for light polarized parallel (perpendicular) to the optic axis, and $\omega_{iA_1}^{TO}$, $\omega_{iA_1}^{LO}$, ω_{iE}^{TO}, and ω_{iE}^{LO} are, respectively, the frequencies of the ith transverse phonon of A_1 symmetry, the ith longitudinal phonon of A_1 symmetry, the ith transverse phonon of E symmetry, and ith longitudinal phonon of E symmetry. The polariton directional dispersion curves spanning the region of interest, $850 < \omega < 1100$ cm^{-1}, have been calculated from Eq. (16) and are shown in Fig. 8. Also shown as solid circles in Fig. 8 are the experimental points for the $\theta = 90°$ polariton measured in the near forward ordinary-ordinary scattering configuration. These points should and do lie on the intersection of the $\theta = 90°$ polariton curves defined by

$$\frac{|\vec{q}|^2}{\omega^2} = \epsilon_\infty^{\parallel}\prod_{i=1}^{3}\frac{(\omega_{iA_1}^{TO})^2-\omega^2}{(\omega_{iA_1}^{LO})^2-\omega^2}\,, \tag{17}$$

with the photon momentum-conservation curves

$$|\vec{k}_L|^2/\omega^2 = \epsilon_\infty^{\perp}\{1-[(\omega_L/\omega)^2-(\omega_L/\omega)]\beta^2\}; \tag{18}$$

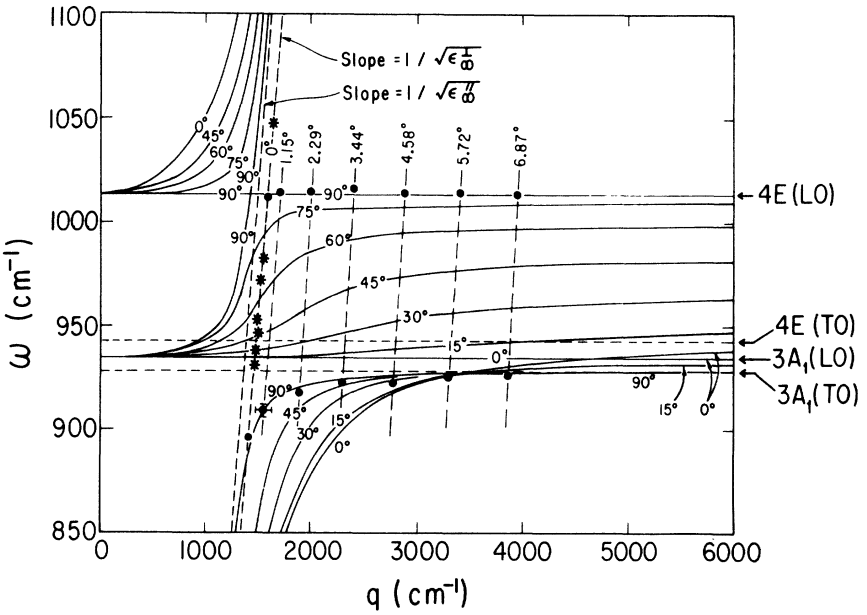

FIG. 8. Polariton directional dispersion curves of $RbClO_3$ for several propagation angles θ. The solid lines are calculated from Eq. (16), while the filled circles are experimental points for $\theta = 90°$. The asterisks indicate CO_2 pump frequencies. The long-dashed lines with angle labels were calculated from Eq. (18) using the scattering angle θ indicated.

here β is the scattering angle. As can be seen from Fig. 8, by judiciously choosing the proper CO_2 photon pump frequencies ω_P, tunable hot polaritons with $\omega \gtrsim 900$ cm^{-1} can be created. This hot polariton tunability is demonstrated in Fig. 9, which again for the purpose of comparison also shows the thermal polaritons. The hot-polariton signals shown in Fig. 9 are much weaker than the maximum signals obtainable at each of the specified pump frequencies.

The relative intensities of the hot polaritons in $RbClO_3$ have been measured as a function of the

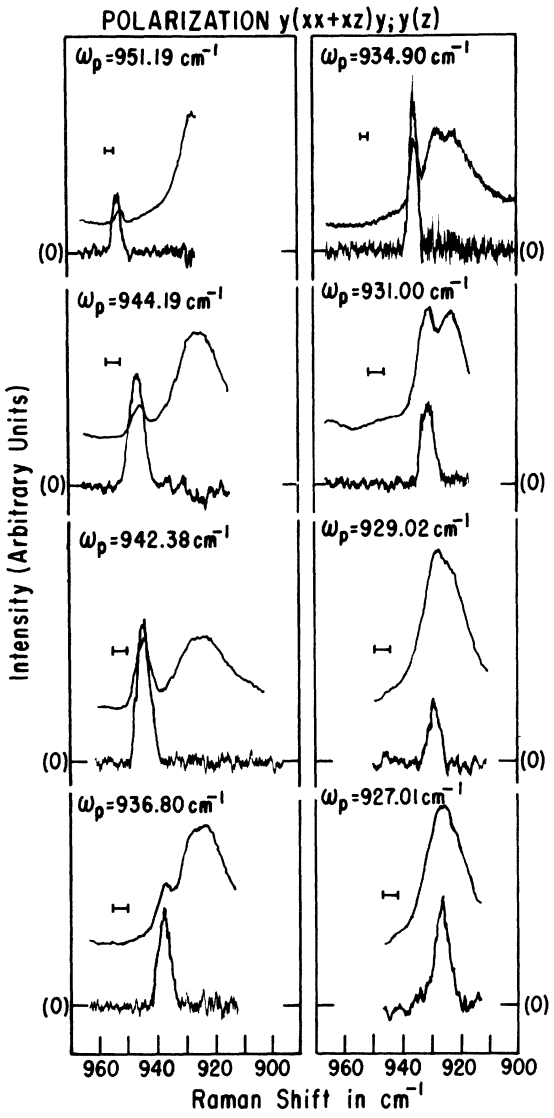

FIG. 9. Frequency tunability of CO_2-laser pumped hot polaritons in $RbClO_3$. The broad thermal-polariton peak remained unchanged, while the frequencies and intensities of the sharp hot-polariton peaks varied as the frequency of the CO_2 laser was changed.

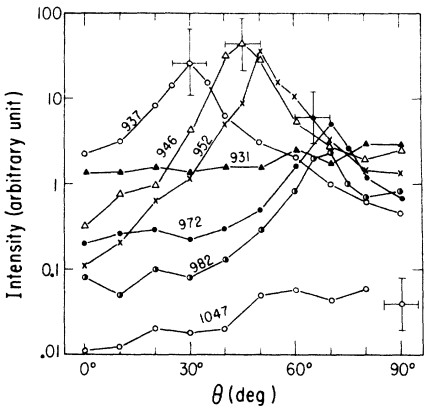

FIG. 10. Hot-polariton (mixed-photon) signal intensity as a function of the CO_2 pump frequency and the polariton propagation angle. The lines connecting the data points corresponding to the same CO_2-laser frequency are drawn to facilitate viewing of the data. The numbers labeling each set of data points specify the CO_2-laser pump frequencies in cm^{-1}.

polariton propagation angle θ for several fixed CO_2 pump frequencies. The observed hot-polariton signals normalized for the CO_2 pump power and the argon-laser probe power are plotted as a function of θ in Fig. 10. The lines connecting the data points in Fig. 10 are drawn to facilitate viewing of the data. Note that at some pump frequencies, e.g., 946 cm^{-1}, the hot-polariton signal varies with propagation angle by more than two orders of magnitude, while at other pump frequencies, e.g., 931 cm^{-1}, the signal exhibits a relatively weak angular dependence. Moreover, most of the curves in Fig. 10 have a well-defined maximum which occurs at a propagation angle that depends upon the CO_2 pump frequency.

In order to explain the phenomena exhibited in Fig. 10 we refer again to Eqs. (6) and (7). The term $|\Delta\vec{k}(\omega_P, \theta)|$ in Eq. (7) is the difference in magnitude between the wave vector of a polariton of frequency ω_P propagating at an angle θ to the optic axis and the wave vector of an ordinary photon of frequency ω_P; i.e.,

$$|\Delta\vec{k}(\omega_P, \theta)| = |(\epsilon_\infty^\perp)^{1/2}\omega_P - |\vec{q}(\omega_P, \theta)|| , \qquad (19)$$

where $|\vec{q}(\omega_P, \theta)|$ is given by Eq. (16). Now the second-order nonlinear susceptibility $d(\omega_P, \theta)$ is not expected to exhibit angle dependent resonances, but rather varies monotonically with θ in the range $0° \leq \theta \leq 90°$. Similarly, the absorption coefficient $\alpha(\omega_P, \theta)$ is a monotonically decreasing or increasing function of θ. The term $n(\omega_P, \theta)$ in Eq. (6) is almost θ independent, since for fixed ω

$$\frac{1}{n^2(\omega, \theta)} = \frac{\sin^2\theta}{n_e^2(\omega)} + \frac{\cos^2\theta}{n_0^2(\omega)} , \qquad (20)$$

where n_e and n_0 are, respectively, the extraordinary and ordinary indices of refraction, and $n_e(\omega) \sim n_0(\omega)$ for $RbClO_3$. On the other hand, the function $|\Delta\vec{k}(\omega_P, \theta)|^2$ is very strongly θ dependent and has a zero at the critical angle $\theta_c(\omega_P)$ for which phase matching is achieved. Thus, on the basis of Eqs. (6) and (7), we expect the intensity of the Stokes (down-converted) and anti-Stokes (up-converted) hot polaritons (mixed photons) to exhibit a peak at the phase-matching angle.

The phase-matching angle can be calculated by substituting Eq. (16) into Eq. (19) and setting the left-hand side of the latter equal to zero. Accordingly

$$\theta_c(\omega_P) = \arcsin\left(\frac{\epsilon''(\omega_P)[\epsilon^{\perp}(\omega_P) - \epsilon_\infty^{\perp}]}{\epsilon_\infty^{\perp}[\epsilon^{\perp}(\omega_P) - \epsilon''(\omega_P)]}\right)^{1/2}, \quad (21)$$

where the dielectric functions $\epsilon^{\perp}(\omega)$ and $\epsilon''(\omega)$ are given by

$$\epsilon^{\perp}(\omega) = \epsilon_\infty^{\perp} \prod_{i=1}^{4} \frac{(\omega_{iE}^{LO})^2 - \omega^2}{(\omega_{iE}^{TO})^2 - \omega^2},$$
$$\epsilon''(\omega) = \epsilon_\infty'' \prod_{i=1}^{3} \frac{(\omega_{iA_1}^{LO})^2 - \omega^2}{(\omega_{iA_1}^{TO})^2 - \omega^2}. \quad (22)$$

The symbols in Eq. (22) retain their previous definitions. In Fig. 11 the function $\theta_c(\omega_P)$ defined by Eq. (21) is plotted as a solid line for $920 < \omega_P < 1020$ cm^{-1}. Also shown in Fig. 11 are the corresponding experimental values of the critical angle determined using several fixed CO_2 pump frequencies. The CO_2 pump frequencies used to record the data of Figs. 10 and 11 are indicated by the asterisks in Fig. 9. Figure 11 not only provides independent proof of the validity of the dielectric functions given in Eq. (22), and therefore of the previously determined TO and LO frequencies of $RbClO_3$, but also clearly confirms our conjecture that the θ dependence of the hot-polariton intensity is dominated by the $|\Delta\vec{k}(\omega_P, \theta)|$ contribution to the coherence length.

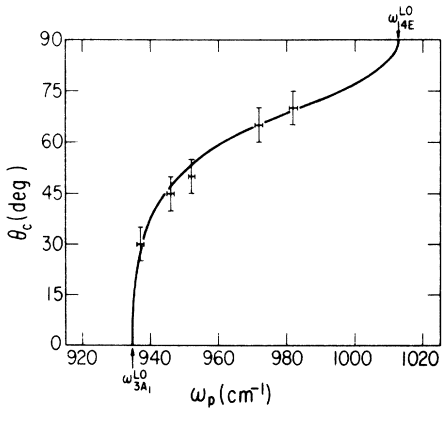

FIG. 11. Phase-matching angle θ_c as function of pumping frequency ω_P. The solid line is calculated from Eq. (21). The data points are obtained from the positions of the peaks in the curves of Fig. 10.

Additional striking confirmation of the $|\Delta\vec{k}|$ term dominance of the angular dependence of $I(\omega_S, \theta)$ is the fact that neither of the curves labeled 931 or 1047 cm^{-1} in Fig. 10 exhibits a critical phase-matching angle, i.e., these curves display no resonances. The absence of a resonance in these particular signal intensity curves is not surprising since, as can be seen from Fig. 8, there is no propagation angle in the range $0° \leq \theta \leq 90°$ at which either of the functions $|\Delta\vec{k}(931 \text{ cm}^{-1}, \theta)|$ or $|\Delta\vec{k}(1047 \text{ cm}^{-1}, \theta)|$ takes on a value of zero or has a local minimum.

As a final point in this section, we note with reference to Fig. 8 that if energy is conserved, a CO_2 photon with $\omega_P = 972$ cm^{-1}, for example, can only pump hot polaritons propagating at $\theta \geq 47°$. Nevertheless, the 972-cm^{-1} intensity curve of Fig. 10 indicates non-negligible hot-polariton signals for $\theta \leq 47°$. This apparent inconsistency arises because we have neglected to include damping terms in Eq. (16). When damping terms are properly included in Eq. (16) the branches of the polariton dispersion curves (for fixed θ) fold back and merge; the energy gaps between them are spanned. It has been pointed out by Barker and Loudon[23] that the resultant gapless polariton dispersion curves are appropriate for ir photons strongly absorbed in the crystal, as are the CO_2 pump photons in $RbClO_3$. Thus the $\omega_P = 972$ cm^{-1} pump photon can generate at least some hot polaritons for any crystal orientation, as is evident from Fig. 10. Clearly, the $\omega_P = 972$ cm^{-1} pump photon is not unique in this regard and was merely chosen in the above discussion for illustrative purposes.

F. Hot-polariton decay products

It is of interest to examine the decay dynamics of the hot polaritons generated by the CO_2 pump laser. Since the CO_2 pulse length is $\sim 10^{-6}$ sec, while the lifetime of the polariton is $\sim 10^{-12}$ sec, a steady-state nonequilibrium hot-polariton distribution is established for the duration of the CO_2 pulse. The hot polaritons are anharmonically coupled to other lattice excitations. Thus, their principal damping mechanism involves a three-phonon interaction which conserves energy and crystal momentum and is governed by the anharmonic Hamiltonian

$$H_3 = \sum_{\vec{q}',\vec{q}''} \sum_{j,j''} (C^{\vec{q}j}_{\vec{q}',j',\vec{q}'',j''} a^{\dagger}_{\vec{q}',j'} a^{\dagger}_{\vec{q}'',j''} a_{\vec{q}j} + D^{\vec{q}j}_{\vec{q}',j',\vec{q}'',j''} a^{\dagger}_{\vec{q}',j'} a_{\vec{q}'',j''} a_{\vec{q}j} + \text{c.c.}) \quad (23)$$

with the constraints

$$\omega_{\vec{q}j} = \omega_{\vec{q}',j'} \pm \omega_{\vec{q}'',j''} \quad (24)$$

and

$$\vec{q} = \vec{q}' \pm \vec{q}'' . \tag{25}$$

In Eqs. (23)–(25), $\vec{q}$, $\vec{q}'$, and $\vec{q}''$ are, respectively, the wave vectors of phonons or polaritons from the j, j', and j'' branches of the dispersion curves, $\omega_{\vec{q}j}$ is the corresponding energy in branch j at wave vector $\vec{q}$ and similarly for $\omega_{\vec{q}'j'}$ and $\omega_{\vec{q}''j''}$ while $C^{\vec{q}j}_{\vec{q}'j',\vec{q}''j''}$ and $D^{\vec{q}j}_{\vec{q}'j',\vec{q}''j''}$ are the anharmonic coupling coefficients for particular damping channels. The + and − signs in Eqs. (24) and (25) correspond, respectively, to the first and second terms in the parentheses of Eq. (23). The former represents the *decay* of a $\vec{q}j$ excitation into a pair of excitations $\vec{q}'j'$ and $\vec{q}''j''$, while the latter represents the *scattering* of a $\vec{q}j$ excitation and simultaneous creation (destruction) of a $\vec{q}'j'$ ($\vec{q}''j''$) excitation.

Although hot-polariton damping products cannot be detected by first-order Raman scattering unless they fortuitously occur at the center of the Brillouin zone, the anharmonic coupling coefficients can, in principle, be measured by studying second-order Raman scattering from various combinations of hot damping products with thermal excitations.[24] In an effort to observe such second-order scattering we have examined under nonequilibrium conditions the Stokes and anti-Stokes Raman spectra of $RbClO_3$. The occupation numbers of the damping products, and therefore the second-order Raman signals to which they contribute, will be modulated by the CO_2 pump beam and should be observable in both the boxcar and photon-counting detection channels. In particular, the second-order scattering signals from combinations involving a hot decay product and thermal excitations as well as from combinations of hot decay products generated in different damping channels will be displaced in energy from the more intense first-order hot-polariton signals.

In Fig. 12 we show an extended Stokes spectrum of $RbClO_3$ pumped with the $p(20)$ line of the CO_2 laser at 944 cm^{-1}. The gain in the boxcar channel has been increased so that now nonequilibrium scattering processes (those modulated by the CO_2 laser pulses) producing signals a factor of 10 000 weaker than the hot-polariton signal at 944 cm^{-1} would be recorded with a signal-to-noise ratio of 1. The spontaneous Raman scattering of the CS_2 index-matching liquid has been labeled in Fig. 12 and is of course unavoidable.[25] Though the intensity of the CS_2 Raman lines is not modulated by the CO_2 laser pulses, the enhanced noise in the boxcar integrator channel at Raman shifts corresponding to those of CS_2 is a manifestation of these lines. As is evident from Fig. 12 we were unable to detect any pumped second-order scattering processes with Raman shifts in the range 700–1000 cm^{-1}. Similar runs have been taken over the range with Raman shifts from −1200 to +1200 cm^{-1} and in the region around ± 1890 cm^{-1} ($\approx \pm 2\omega_P$). No signal was observed other than the strong first-order signals at ± 944 cm^{-1}.

At room temperature, the dominant mechanism for optical polariton or optical phonon damping is scattering off of thermal phonons. There are a multitude of allowed scattering channels [i.e., those three phonon processes obeying Eqs. (24) and (25)] linking thermal acoustic phonons to hot polaritons. Thus, the increase in the occupation number of the phonon damping products in each scattering channel is apparently not large enough to facilitate observation of the modulated second-order Raman spectrum. Clearly, by cooling the $RbClO_3$ sample to temperatures in the liquid-helium range, the population of thermal phonons could be significantly reduced and the modulated second-order Raman signal correspondingly enhanced. Unfortunately, the immersion technique for index matching[7] is

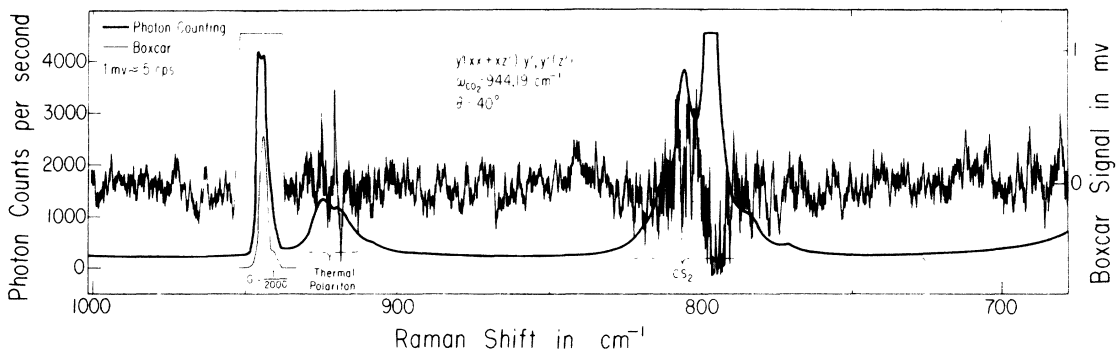

FIG. 12. High gain scan of boxcar channel in search of hot-polariton damping products. The dip in the peak of the 944-cm^{-1} hot polariton recorded in the photon-counting channel is artificial and results from saturation of the counting system engendered by the low (0.0023) duty factor of the Q-switched CO_2 laser. The effective count rate (which is equal to be observed count rate, ~4000 cps, divided by the duty factor) was 1.7×10^6 cps.

presently limited to temperatures $\geq -100\,^{\circ}$C. It is therefore not possible at this time to achieve at liquid-helium temperature the necessary index-matching condition required for proper phase matching, and efficient photon-up or down conversion.

Careful examination of the polariton directional dispersion relation given in Eq. (16) reveals that there is a unique propagation direction $\theta = 36^{\circ}$ at which the $3A_1(\mathrm{LO}) - 4E(\mathrm{LO})$ polariton with $\omega = 972$ cm^{-1} can decay into a subharmonic pair of $3E(\mathrm{TO})$ zone-center phonons at $\omega = 486$ cm^{-1}.[6] Thus we have used the $p(14)$ 972-cm^{-1} line of the CO_2 laser to pump the $\theta = 36^{\circ}$ $3A_1(\mathrm{LO}) - 4E(\mathrm{LO})$ polariton and have searched the boxcar detection channel extensively for CO_2-modulated *first-order* Raman scattering at a frequency shift of 486 cm^{-1}. The modulated first-order Raman signal from the decay products of the optically pumped hot polaritons can be expected to be two- to three-orders-of-magnitude more intense than the second-order Raman signal. However, as can be seen from Figs. 10 and 11, the phase-mismatch at $\omega_P = (972$ cm^{-1}, $\theta = 36^{\circ})$ is significant enough to reduce the conversion efficiency by about two orders of magnitude below its maximum value. The net effect is to again render the hot-polariton damping products unobservable.

IV. CONCLUSIONS AND SUMMARY

The mixing of visible and ir photons on $RbClO_3$ has been measured and analyzed using the second-order nonlinear susceptibility tensor and the Raman tensors for polar phonons. The polarization properties of the mixed (Raman-scattered) photons are predicted accurately by both tensor analyses, as are various features of the intensity of the mixed or scattered photons. In particular, it is found that the intensity of photons Raman scattered from optically pumped hot polaritons varies by three orders of magnitude as the polariton frequency and propagation direction are changed, and is a maximum at the critical propagation angle for which phase matching is achieved. The dependence of the critical propagation angle on the ir pump frequency has been calculated and measured. Agreement between theory and experiment is excellent.

Although steady-state nonequilibrium hot-polariton occupation numbers corresponding to equilibrium sample temperatures in excess of $10^{11}\,^{\circ}$K have been produced, no first- or second-order Raman scattering from the hot-polariton anharmonically coupled damping products has been observed. The observation of such damping products is precluded by the inability to apply to $RbClO_3$ crystals of poor optical quality, the immersion technique for index matching at temperatures in the liquid-He range. Therefore, the thermal phonons which dominate the hot-polariton damping processes cannot be effectively quenched in $RbClO_3$. Because high-quality single crystals of α quartz are readily available, mixing of ir and visible light in that material can be achieved at low temperatures without the need for index matching. The room-temperature hot polariton Raman signals for *non-collinear* mixing of CO_2 and argon-laser light in α quartz are almost as intense as the peak signals obtained from $RbClO_3$.[26] We plan to extend the α-quartz measurements to 4 $^{\circ}$K in order to observe hot-polariton decay products in that material.

ACKNOWLEDGMENTS

Thanks are due to R. J. Kobliska for constructing the CO_2 laser used in this experiment and for useful discussions. We also thank N. Strahm for bringing to our attention Refs. 2 and 3.

---

*Research supported by the U. S. Atomic Energy Commission under Contract No. AT (11-1) 2126. It has also benefited from the general support of Materials Science at the University of Chicago by the National Science Foundation.

[1]D. M. Hwang and S. A. Solin, Solid State Commun. 13, 983 (1973).

[2]W. L. Faust and C. H. Henry, Phys. Rev. Lett. 17, 1265 (1966).

[3]W. L. Faust, C. H. Henry, and R. H. Eick, Phys. Rev. 173, 781 (1968).

[4]R. W. G. Wycoff, *Crystal Structures*, 2nd ed. (Wiley, New York, 1964), Vol. I, Chap. III.

[5]Reference 4, Vol. II, Chap. VIIA.

[6]D. M. Hwang and S. A. Solin, Phys. Rev. B 7, 843 (1973).

[7]D. M. Hwang and S. A. Solin, Appl. Phys. Lett. 20, 181 (1972).

[8]D. M. Hwang, R. J. Kobliska, and S. A. Solin (unpublished).

[9]*The Handbook of Chemistry and Physics*, 51st ed., edited by R. C. Weast (The Chemical Rubber Publishing Co., Cleveland, 1970).

[10]H. Swanson, N. Gilfrich, M. Cook, R. Stinchfield, and P. Parks, Natl. Bur. Stds. Circ. No. 539 (unpublished), Vol. 8, p. 47.

[11]T. C. Damen, S. P. S. Porto, and B. Tell, Phys. Rev. 142, 570 (1966).

[12]J. F. Nye, *Physical Properties of Crystals* (Clarendon, Oxford, England, 1957).

[13]T. Y. Chang, Opt. Commun., 2, 77 (1970).

[14]R. Loudon, Adv. Phys. 13, 423 (1964).

[15]*Handbook of Lasers*, edited by R. C. Weast (The Chemical Rubber Publishing Co., Cleveland, 1971), p. 491.

[16]A. Yariv, *Iniroduction to Quantum Electronics* (Wiley, New York, 1967), p. 342.

[17]See, e.g., J. F. Scott and S. P. S. Porto, Phys. Rev. 161, 903 (1967).

[18]R. Loudon, in *Proceedings of the International Conference on Light Scattering Spectra of Solids*, edited by

G. B. Wright (Springer-Verlag, New York, 1969), p. 25.
[19]S. A. Solin and A. K. Ramdas, Phys. Rev. B 1, 1687 (1970); also R. J. Kobliska and S. A. Solin, Phys. Rev. B 8, 756 (1973).
[20]The reflectivity was calculated from the complex dielectric functions of $RbClO_3$ given in Ref. 6.
[21]D. M. Hwang and S. A. Solin (unpublished).
[22]G. Merten, Phys. Status Solidi 25, 125 (1968).
[23]A. S. Barker, Jr and R. Loudon, Rev. Mod. Phys. 44, 18 (1972).
[24]D. M. Hwang, R. J. Kobliska, and S. A. Solin, in *Proceedings of the Second International Conference on Light Scattering in Solids*, edited by M. Balkanski (Flammarion, Paris, 1971), p. 260.
[25]S. Bhagavantam, Phys. Rev. 39, 1020 (1932).
[26]D. M. Hwang and S. A. Solin (unpublished).